DOI: 10.11835/j.issn.2096-6717.2022.002
开放科学(资源服务)标识码 OSID:

Interfacial bonding characteristics between quartz sand supported nano-TiO_2 functional aggregates and cement paste

WANG Gongxun[a,b], *LI Xiong*[a], *DENG Jing*[a], *ZHU Mingqiao*[a,b], *QU Feng*[a]
(a. School of Civil Engineering; b. Hunan Engineering Research Center for Intelligently Prefabricated Passive House, Hunan University of Science and Technology, Xiangtan 411201, Hunan, P. R. China)

Abstract: Photocatalytic cement-based material is one of the research hotspots of advanced building functional materials, but TiO_2 cement-based composites prepared by the traditional internal mixing method have low effective utilization rate of TiO_2 and poor economic benefits. To solve this problem, cement mortar with quartz sand supported TiO_2 (QST) aggregates were prepared and the effects of the QST aggregates on the drying shrinkage performance of the cement mortar was studied. The interfacial bond strength between the QST aggregates and the cement stone was measured using the pull-out strength method. The effects of the nano TiO_2 on the hydration products and pore structure of the interfacial transition zone (ITZ) between the aggregates and the cement stone were studied via SEM, EDS and MIP methods. Compared with ordinary quarz sand aggregates, the QST aggregates can reduce the drying shrinkage of the cement mortar and improve the interfacial adhesion between the aggregates and the cement stone. The nano TiO_2 that was loaded onto the surface of the aggregates promotes the hydration of the cement paste, reduces the enrichment of $Ca(OH)_2$ in the ITZ, and refines the pore structure of the ITZ between the cement stone and the aggregates.

Keywords: functional aggregate; interfacial bond strength; interfacial transaction zone (ITZ); hydration product; pore structure

负载纳米 TiO_2 石英砂功能集料-水泥石的界面粘结性能

王功勋[a,b],李雄[a],邓静[a],祝明桥[a,b],屈锋[a]
(湖南科技大学 a.土木工程学院; b.湖南省智慧建造装配式被动房工程技术研究中心,湖南 湘潭 411201)

摘　要:光催化水泥基材料是先进建筑功能材料的研究热点之一,但传统内掺法制备的 TiO_2-水泥基复合材料中 TiO_2 有效利用率低、经济效益差。针对此问题,采用负载法制备纳米 TiO_2 功能集料(QST),并将 QST 集料负载于普通水泥砂浆表面。研究 QST 集料对水泥砂浆干缩性能的影响,通过拉拔法测试 QST 集料与水泥石的界面粘结力;采用 SEM、EDS、MIP 等微观测试方法,研究纳米 TiO_2 对集料-水泥石界面过渡区水化产物、孔结构的影响。结果表明:与普通石英砂集料相比,表面负载纳米 TiO_2 的石英砂功能集料可减少水泥砂浆的干缩,提高集料-水泥石的界面粘结力。在 QST 集料-水泥石的界面过渡区,纳米 TiO_2 促进了水泥浆体的水化,减少了界面过渡区 $Ca(OH)_2$ 的富集,细化并改善了界面过渡区的孔结构。

关键词:功能集料;界面黏结力;界面过渡区;水化产物;孔结构
中图分类号:TU528.01　　**文献标志码:**A　　**文章编号:**2096-6717(2024)02-0176-12

Received: 2021-08-24
Foundation items: the State Scholarship Fund (No. 201709480008); Hunan Province Education Scientific Project (No.19A164); National Undergraduate Research and Creative Experiment Project (No. S202010534006)
Author brief: WANG Gongxun (1979-), PhD, associate professor, main research interest: new construction materials, E-mail: wanggx@hnust.edu.cn.

1 Introduction

Photocatalytic properties of nano-TiO_2 have important and practical significance for air pollution control[1], therefore, photocatalytic cement-based materials represent a critical industrial opportunity. Nowadays, many researchers have focused on the photocatalytic properties of nano-TiO_2 cement-based materials used in buildings and pavement[2-5]. Some investigations have concentrated on the effects of the photocatalyst environment, such as humidity[6], and illumination intensity of photocatalytic efficiency[7]. Similarly, the effects of nano-TiO_2 on the hydration of cement have also been studied[8-10]. Despite the effectiveness of TiO_2 as a photocatalyst, its use in practical applications is relatively small. The common application method in construction is to mix nano-TiO_2 directly into the cement paste or concrete in Fig. 1(a)[11-14]. Since photocatalysis is a surface phenomenon, influenced by the chemistry of the immediate environment, the photocatalytic effects of nano-TiO_2 can only be effectively activated under exposure to ultraviolet radiation[15-16]. When TiO_2 is covered by cement, only a small portion of the TiO_2's surface is exposed in the surface layer. This results in a waste of the utilization and economic effectiveness of the relatively expensive nano-TiO_2. The concrete surface must be engineered to maximize the photocatalysts accessibility (to reactants) and activation (illumination); therefore, increasing the effective exposure area of the nano-TiO_2 and improving the photocatalytic efficiency of the nano-TiO_2. These are important means in order to solve the above problems and are also an important research direction for nano-TiO_2 cement-based composite functional materials[17-19].

Wang, et al.[20] proposed a surface mounting for a functional aggregate loaded with nano-TiO_2 in Fig. 1(b) to address these problems. Their research focused on the preparation process and the photocatalytic performance of the loaded nano-TiO_2 aggregate mortar. The results showed that the photocatalytic efficiency of the loaded TiO_2 aggregate mortar is considerably higher than that of the traditionally dispersed nano-doped TiO_2 mortar[21-22]. The embedding depth (exposed area) of the loaded TiO_2 aggregates directly affects the photocatalytic efficiency and the bonding strength between the aggregates and the mortar[23-24].

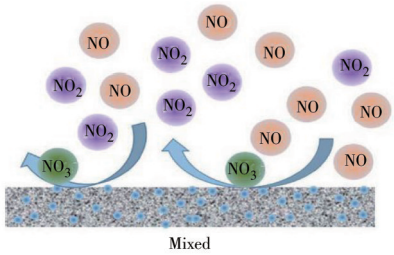

(a) Conventional TiO_2 dispersions in concrete

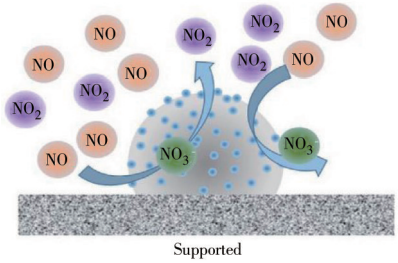

(b) Surface-mounted TiO_2-aggregate composites on photocatalytic concrete

Fig. 1　TiO_2 mixed directly into the concrete and quartz sand supported TiO_2 (QST)[20]

Under normal service conditions, the interface between the loaded TiO_2 aggregates and the cement stone may be considered the weak zone due to the influence of environmental factors such as moisture movement potentially leading to phase precipitation[25], and expansive crystallization[26], through variations in temperature, humidity, freezing, and thawing[27-28]. Nano-TiO_2 has no pozzolanic activity and does not directly participate in the hydration reaction of the cement[29-30]; however, its nano particles contain high surface area sites for the nucleation of cement hydration products promoting the hydration of cement, enhancing space filling, and indirectly influencing the bonding characteristics of the interface[31-34].

This work focuses on the bond properties of the interface between loaded nano-TiO_2 aggregates and cement under the conditions of dry shrinkage, dry and wet cycle, and studies the microstructure of the interface region between the aggregates loaded with nano-TiO_2 and the cement stone in order to better understand the role of nano-TiO_2 on the interface between the aggregates and the cement.

2 Experimental details

2.1 Raw materials

The aggregates used as TiO_2 supports are ISO standard sand (ISO 679: 2009) produced from Leucate, France (designated FS). The particle size of the quartz sand is 1-2 mm. Titanium tetra-isopropoxide (TTIP, 99.9%), acetic acid (CH_3COOH, 99.6%), absolute ethanol (C_2H_5OH, 99.9%), NaOH (sodium hydroxide, 0.1 mol/L), were purchased from Sigma-Aldrich. Deionized water (18.2 MΩ·cm) was used throughout the TiO_2 hydrosol preparation process.

The sand and CEM I 52, 5N (PC) used to produce the mortar conforms to BS EN 196-1 (BSI, 2005) and BS EN 197-1 (BSI, 2011), respectively.

2.2 Methods

2.2.1 Preparation of quartz sand supported TiO_2 (QST) aggregates

The TiO_2 hydrosol preparation process and the QST aggregate preparation followed the method previously described by reference [11]. The main steps are summarized here. In order to activate the quartz surface, the sand aggregates were first treated with 0.1 mol/L NaOH for 24 h followed by washing with deionized water three times. The activated sands were then immersed in anatase TiO_2 hydrosol suspensions for 5 minutes at room temperature. The resulting composites were then separated by filtration and dried at 105 ℃ for 30 minutes. The process above was repeated for the required 6 coating cycles. In the final step, all samples were dried at 105 ℃ for 24 hours, then washed three times using deionized water before the final drying step. In reference [11], Yang , et al. confirmed that the TiO_2 loading increases with the number of coating cycles. This translates to a loading thickness (d) of up to 1 850 nm at a TiO_2/SiO_2 mass fraction of 0.61% after 6 coating cycles. Fig. 2 shows an SEM micrograph of the QST aggregates. TiO_2 can be observed on the aggregate surface as agglomerated nano-TiO_2.

2.2.2 Preparation of QST cement mortar

Portland cement-sand-water were mixed in a mass ratio of 1∶3∶0.5 according to the procedures described in BS EN 196-1:2005[35]. Mortar samples with a size of 100 mm×50 mm×50 mm were prepared for the drying shrinkage test. The process to prepare the aggregate exposed mortar is as follows:

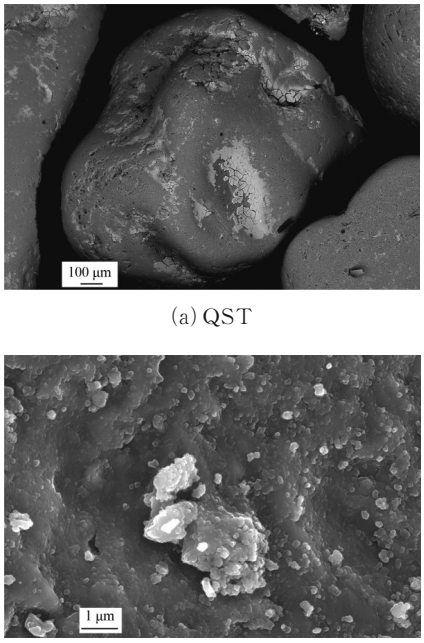

(a) QST

(b) TiO_2

Fig. 2 SEM images of QST and TiO_2 supported on the surface of QST

1) Aggregates were sprinkled onto a 50 mm wide adhesive tape to ensure a specific amount of single layer aggregates were mounted to each test sample, the coated sand was pre-laid onto a 100 mm long adhesive tape. Typically, this enables 9 g to 10 g of the coated sand to be mounted.

2) Aggregate mounting: the aggregate-coated tape was then placed onto the freshly as-cast surface of the mortar substrate and pressed into the surface under the load of a concrete block to give the specified aggregate exposure (via the depth of embedding). The samples were demoulded after 24 hours and cured under standard conditions in water for 7 days. The tape was then peeled off from the hardened mortar, leaving a single layer of aggregates exposed onto the top surface of the mortar samples.

2.2.3 Measurement

1) Drying shrinkage test of the mortar. Length l_x and mass m_x of the samples prepared for the drying shrinkage test were measured at various ages (x days) under 20 ℃ and 50% RH condition; x is the curing day since the samples were moved into the curing room (x=0, 1, 4, 7, 14, 21, and 28).

2) Dry-wet cycle test of the mortar. After applying the aggregate coating, the samples were

demoulded after curing at 20 ℃ and 100% RH conditions for 24 hours, and further cured in water for 6 days. Then, the samples were dried at 20 ℃ for 24 hours and the copper heads were pasted onto the sample ends using Araldite resin. When the resin hardened after 30 minutes, the samples were moved to the curing room (20 ℃, RH=50%) and the initial length l_0 and the mass m_0 were measured before they were immersed in water at 20 ℃. The dry-wet cycle (immersion for 8 hours, followed by drying at 60 ℃ for 8 hours) was repeated 200 times, after which the final length and the mass of sample was measured.

3) Pull-out strength test between the QST aggregates and the cement paste. Samples were dried at 20 ℃ for 24 hours before the pull-out strength test was performed, as follows: Araldite resin was applied to the mortar and test equipment dolly. The samples were scratched prior to pressing the mortar and the dolly together in Fig. 3. After the resin set, a direct tensile load was applied to measure the bonding strength between the aggregates and the cement paste. The loading rate of the pull-out strength test was 20 psi/s.

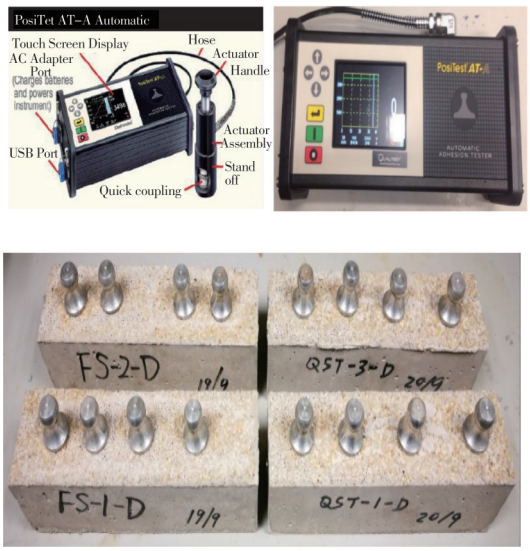

Fig. 3　Posi-Test AT-A instrument for pull-out test and dolly glued on the surface of mortar

4) Characterization. The samples' morphology was observed using a scanning electron microscope (SEM, Zeiss EVO MA10) equipped with an energy dispersive X-ray spectrometry (EDS, Oxford INCA) for elemental composition analyses.

The mercury intrusion porosimetry (MIP) method was used to analyze the pore structure of the cement paste samples via the equipment of the AutoPore Ⅳ 9510, Micromeritics. The boundary conditions of the pressure and the pore sizes of the MIP equipment are 0.10-61 000 psia and 5-300 000 nm, respectively.

3　Results and discussion

3.1　Drying shrinkage ratio

The potential effects of nano-TiO_2 on the hydration process and pore structure in the ITZ of QST and cement paste, along with its super-hydrophilic properties, could have a significant impact on the water transport properties in the ITZ. However, another factor to consider is the consequences of the interfacial bonding strength between the aggregates and the mortar when considering the relative movement of the porous cement matrix and the dimensionally stable aggregates. Based on the influences of nano-TiO_2 on the hydration properties of the cement-based materials, the drying shrinkage of the hardened cement paste has been investigated and discussed.

Fig. 4 shows the variations in the sample's mass of various mortar samples coated by French sand (FS) and quartz sand supported TiO_2 (QST) aggregates. Fig. 5 is the curve of the drying shrinkage rate of different mortar samples coated by French sand (FS) and quartz sand supported TiO_2 (QST) aggregates.

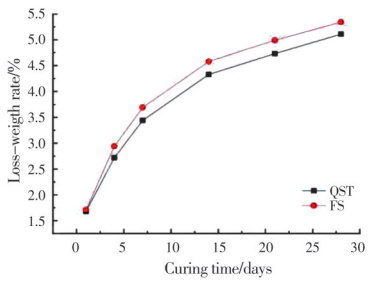

Fig. 4　Curve between loss weight rate and curing time of mortar samples

It can be concluded that the weight loss of the FS mortar was higher than that of the QST mortar as shown in Fig. 4. In Fig. 5, the drying shrinkage rate of the QST mortar is smaller than that of the FS mortar. The results match that of Zhang, et al. [36], which concluded that the addition of nano-TiO_2 can reduce the water loss of the sample. Shimomura, et al. [37], Maekawa, et al. [38], and Shimomura [39],

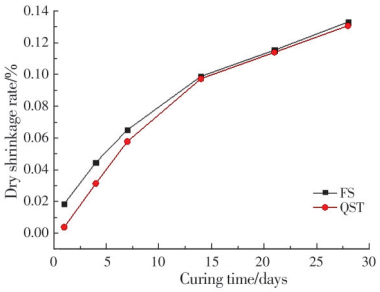

Fig. 5 Curve between the drying shrinkage rate and the curing time of the mortar samples

proposed a micromechanical model of drying shrinkage behavior, which was based on pore size distribution and thermodynamic behavior of the water within the pores. Part of the model involved computation of the parameter r_s, defined as the radius of the pores where the meniscus forms, i. e., the pores whose radii are smaller than r_s are assumed to be filled with liquid water while pores larger than this are dry. As the drying progresses, the parameter r_s decreases. The researchers hypothesized that the smaller the parameter r_s, the larger the capillary tensile forces at the meniscus (the interface between water and air), hence the higher the resulting shrinkage [40].

Drying shrinkage of cementitious materials may be due to a higher volume of mesopores causing a higher capillary stress of the water meniscus developed within the capillary pores of the paste, resulting in a higher level of drying shrinkage. Nano-TiO_2 particles present pore refinement effects on the cement-based materials; thus, resulting in a much denser microstructure and a lower shrinkage value [36,41].

3.2 Pull-out strength of the mortar

Pull-out strength of the FS and QST mortar under different curing conditions are shown in Fig. 6.

It is observed that the pull-out strength of the QST mortar is higher than that of the FS mortar

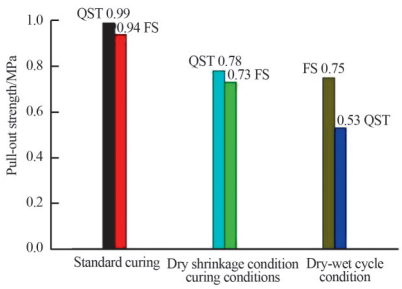

Fig. 6 Pull-out strength of the mortar samples under different curing conditions

during the standard curing and the drying shrinkage conditions; however, the contrary result is observed under the dry-wet cycle condition. Regarding the hygroscopic properties, the increase of TiO_2 content leads to mortar with higher open porosity and water absorption coefficients [42]. When the samples were in the dry-wet cycle conditions, the QST mortar absorbed more water and caused a higher open porosity in the bonding area between the QST aggregates and the cement paste; thus, lowering the bonding strength between the QST and the cement paste.

3.3 Microstructure analysis

3.3.1 SEM of the QST aggregates dropped from the surface of the mortar

Fig. 7 shows the QST dropped from the surface of the mortar. Hydration products of the binding area between the QST aggregates and the cement paste can be observed by SEM in Fig. 7(b) and (c).

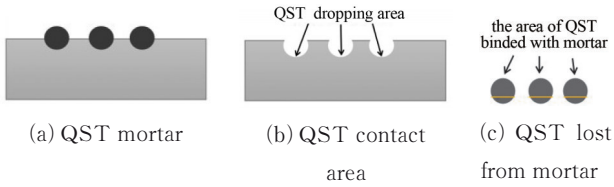

Fig. 7 Diagram of QST dropped from the surface of the mortar

Fig. 8 shows an SEM micrograph of a QST particle dropped from the surface of the mortar and focused on a region originally in contact with the mortar.

Fig. 8(a) shows a QST aggregate partially covered by cement hydration products. Nano-TiO_2 agglomeration on the surface of QST is observed in Fig. 2(a) and is not found in Fig. 8(a), indicating that the bonded interface saturated the SiO_2 surface. The chemical bonding strength between TiO_2 and the quartz aggregates is stronger than that of TiO_2 and the cement paste. Ti—O—Si chemical linkages are confirmed in the reference [11], and TiO_2 accumulation has been shown on the surface in multiple agglomerated layers. Many needle-like hydration products (AFt) are observed in Fig. 8(b); it is deduced that the degree of cement binding with the surface of QST is high. This is due to the nucleation effect of the TiO_2 accelerating the cement hydration

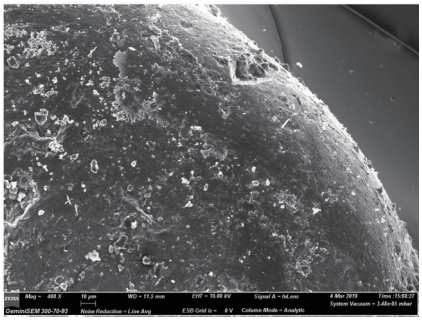

(a) QST dropped from the surface of the QST mortar

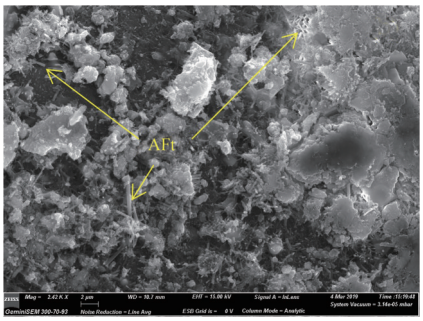

(b) Hydration products of Aft on the surface of QST

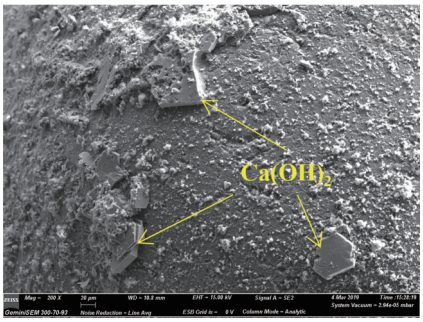

(c) Hydration products of $Ca(OH)_2$ on the surface of QST

Fig. 8　SEM images

process. In Fig. 8(c), hexagonal plate hydration products are observed on the surface and are typical of $Ca(OH)_2$. The size of these $Ca(OH)_2$ plates and their proximity to each other suggest regions of fluid filled porosity prior to failure, in which the crystallization of $Ca(OH)_2$ could have presented regions prone to cleavage and mechanical weakening.

Fig. 9 shows an SEM micrograph and EDS of a vacated site on the mortar, originally occupied by a QST particle.

Fig. 9(a) shows the recess as well as the massive crystals formed by $Ca(OH)_2$ and were observed on the cement coated QST surface. Fig. 9(b) shows analytical locations and Fig. 9(c) is the EDS elements spectra of the vacated area on the surface of the mortar. The primary elements within this area are Si, O, Ca, Al, and C with only a small quantity of Ti. It can be deduced that some TiO_2 has debonded from the aggregates, indicating that the bonding strength between TiO_2 and the quartz is not uniform (as previously indicated by Yang, et al. for coatings of various thicknesses)[11]. In Fig. 2(a), a non-uniform distribution of TiO_2 on the surface of the quartz aggregates are observed, with the possibility of multiple TiO_2 layers. In reference [11], Yang, et al. discussed the weaker binding of TiO_2 in thicker layers but emphasizes the stability of the monolayer closest to the surface.

3.3.2　EDS of the ITZ between the aggregates and the cement paste

In order to identify the effects of the nano-TiO_2

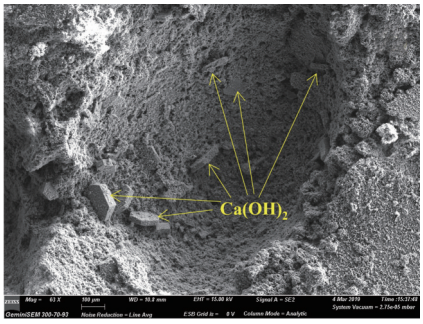

(a) SEM image of hydration products of $Ca(OH)_2$ in QST-dropping area

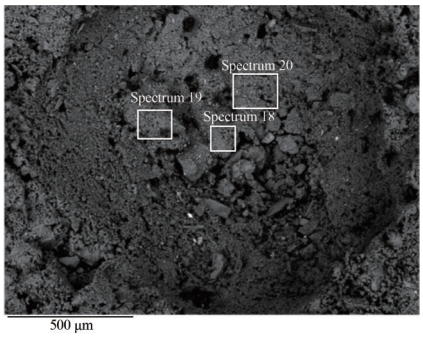

(b) SEM image of QST-dropping area

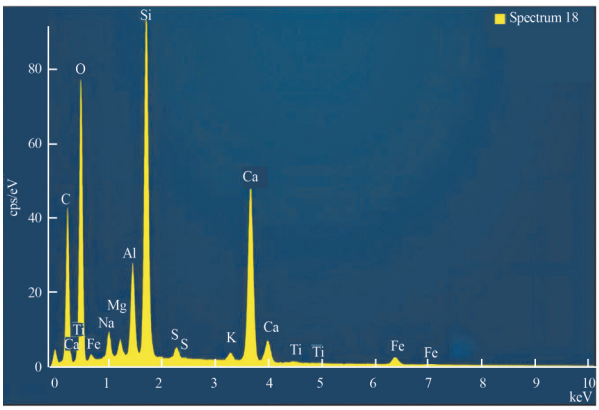

(c) EDS elements spectra of QST-dropping area

Fig. 9　SEM image and EDS elements spectra

on the microstructure of the interface between the QST and the mortar, SEM images of the FS and the QST mortar were obtained. Fig. 10 are the EDS spectra of the ITZ between the FS and the cement paste.

Fig. 10(a) shows the interface and the surrounding regions indicating a significant separation between the FS and the cement. Some separation regions contain a Ca-rich brightly colored substance identified as $CaCO_3$. It is proposed that $Ca(OH)_2$ produced in the interface between the FS aggregates and the cement paste during the cement hydration process is readily carbonated within the open/porous microstructure.

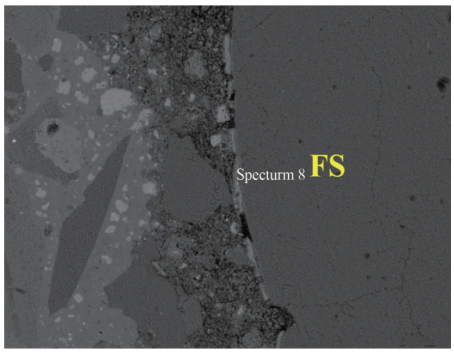

(a) SEM image of ITZ between the FS and the cement paste

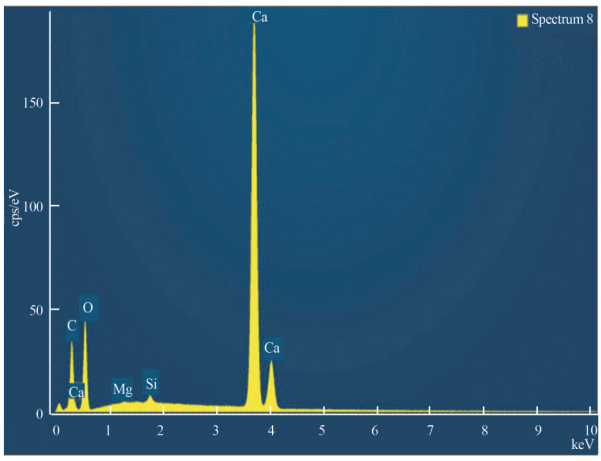

(b) EDS elements spectra of ITZ-dropping area

Fig. 10 SEM image and EDS elements spectra of the ITZ between the FS and the cement paste

Fig. 11 shows the direction of a line-scanning analysis across the interface between the FS and the cement paste.

Fig. 11(a) shows the scanning line position and Fig. 11(b) is a partially enlarged detail of the scanning line area. The microstructure of the gap between the FS particles is loose in Fig. 11(a) and (b). The elemental profiles (Fig. 11(c) to (h)) indicate the presence at the interface of the primary chemical constituents of the cement, indicating that the aggregates have been squeezed into the mortar forcing the extrusion of the cement fragments into the inter-aggregate region.

Fig. 12 shows the direction of a line-scanning analysis made across the interface between the QST and the cement paste.

Compared to Fig. 10(a), the ITZ between the QST particles and the cement paste is more compact in Fig. 12(a) and (b). In Fig. 10(a), a significant separation exists between the FS and the cement. In these separations, many pores and Ca-rich substances are identified as $CaCO_3$ (in Fig. 10(b)) and were found between the FS aggregates and the cement paste. However, an enlargement of Area 1 (Fig. 12 (a)) confirms a denser microstructure compared with the FS system within the interface region. A large content of Ti (Fig. 12 (c) indicates a layer of TiO_2 which is to be expected on the surface of the aggregates. In Fig. 12(d), the content of Ti reduces significantly, Si increases, and the ratio of Ca to Si is minimal; thus, showing that the primary composition within this area is probably SiO_2 as well as cement hydration products. The compositions in Fig. 12(f) are similar to those in Fig. 12(d). In Fig. 12(e), Ti does not exist, the content of Si is significantly reduced, Ca increases, and the ratio of Ca to Si is high. It shows that the primary composition within this area is more than likely the cement hydration products.

Compared to Fig. 11, the microstructure of the ITZ between the QST and the cement paste is more compact than that of the FS. The micrographs and the elemental analysis indicate a higher level of pore filling by the hydration products at the QST-cement paste interface region than in the FS system. It can be deduced that TiO_2 coated on the surface of the aggregates improves the degree of hydration of the cement and makes the microstructure and the interface between the aggregates and the cement

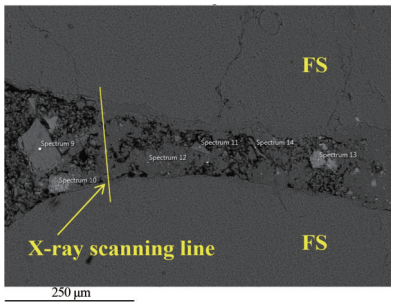

(a) SEM image of the interface region between the FS and the cement paste

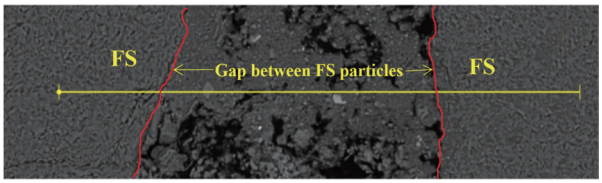

(b) SEM image of gap between FS particles

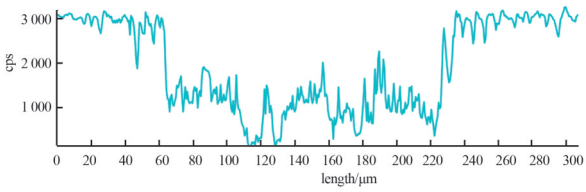

(c) the Si element content of the gap between FS particles

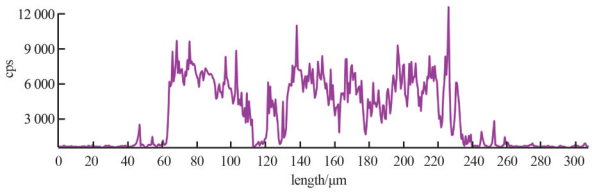

(d) the Al element content of the gap between FS particles

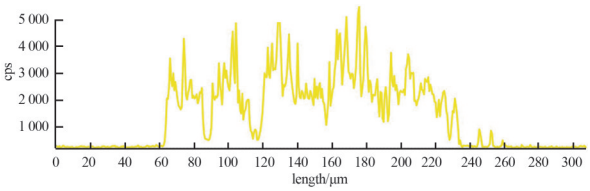

(e) the Ca element content of the gap between FS particles

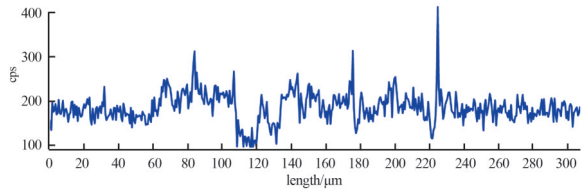

(f) the Ti element content of the gap between FS particles

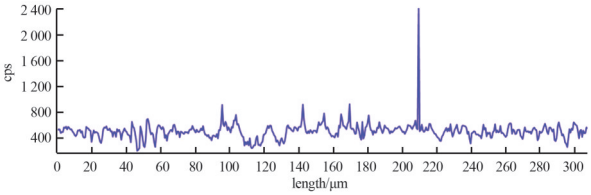

(g) the S element content of the gap between FS particles

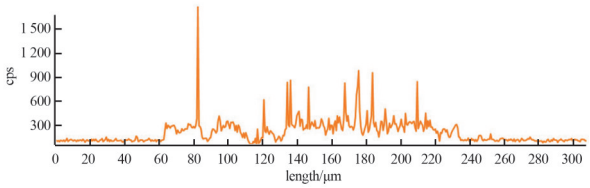

(h) the Fe element content of the gap between FS particles

Fig. 11　Line-scanning analysis of the interface region between the FS and the cement paste

denser. Hence, the pull-out strength of the QST-cement paste is higher than that of the FS-cement paste under standard curing and drying shrinkage curing conditions in Fig. 6. However, the contrary results under the dry-wet cycle conditions still need further investigation.

Fig. 13 is the line-scanning analysis of the ITZ between the QST and the cement paste.

Fig. 13(a) shows the scanning line position across the QST particle and the ITZ. Fig. 13(b) is a partially enlarged detail of the scanning line area. According to Fig. 13(f), it can be concluded that a layer of TiO_2 within the line-scanning range from 4 μm to 8 μm exists in Fig. 13(b). It can again be concluded that the interface between the QST and the cement paste is filled with the hydration products of cement as seen in Fig. 13. The white particle crossed by the scanning line has a high content of Ca, Al, and Fe, but a lower content of S, which is probably the hydration products of C_4AF. The needle-like hydration products are AFt because they have a higher Ca, S, and Al content.

3.3.3　Mercury intrusion porosimetry (MIP)

The most probable and average pore sizes are important parameters of the cement pore structure and characterize the pore structure of the overall situation. The pore size distribution of the ITZ between the various aggregates and the cement paste is shown in Fig. 14. Table 1 is the pore structural index of the ITZ of the QST-cement paste and the FS-cement paste.

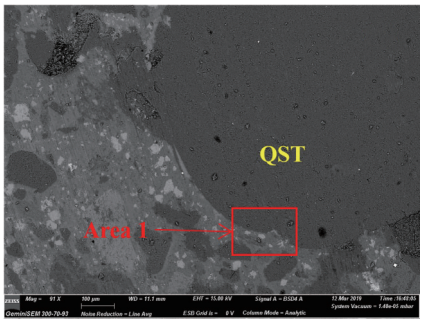

(a) SEM image of the ITZ between QST and cement paste

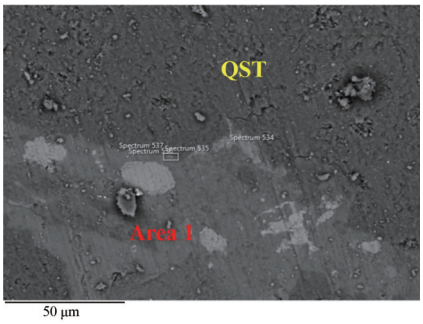

(b) SEM image of spectra areas

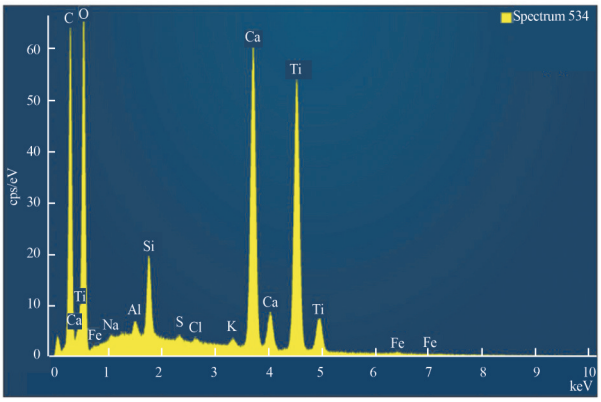

(c) EDS elements spectra of 534 area

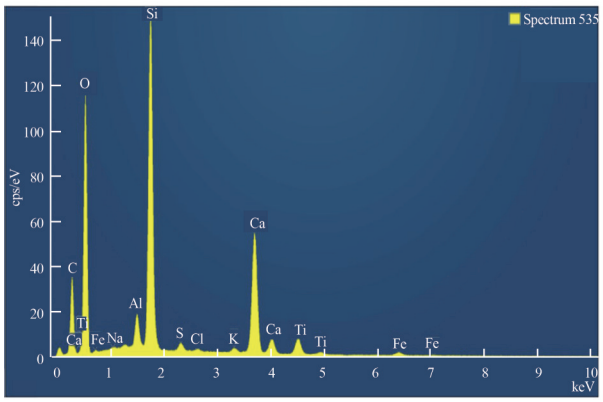

(d) EDS elements spectra of 535 area

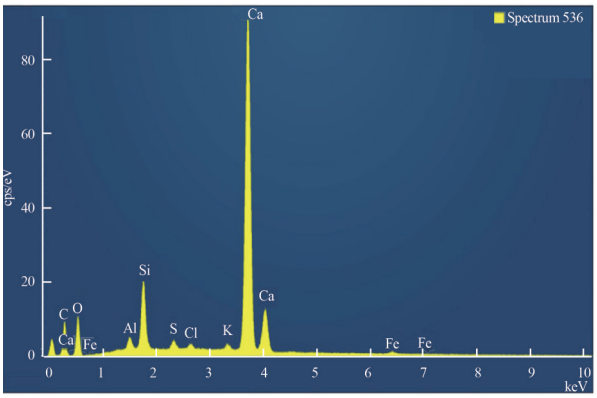

(e) EDS elements spectra of 536 area

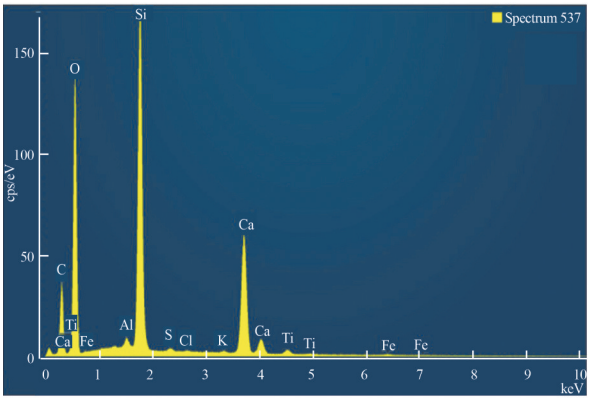

(e) EDS elements spectra of 537 area

Fig. 12 SEM image and EDS elemental spectra of the ITZ between the QST and the cement paste

Table 1 Pore structural index of the ITZ of the QST-cement paste and the FS-cement paste

Sample	Most Probable pore diameter/nm	Porosity/%	Average pore diameter/nm	Pore size distribution/nm			
				>200	50-200	20-50	<20
QST	41.26	17.30	19.98	11.33	21.61	30.76	36.3
FS	50.33	14.48	23.12	14.0	17.49	30.33	38.18

It shows that the most probable pore diameter of the ITZ between the QST and the cement paste is approximately 41.26 nm, which is smaller than that of the FS. The total porosity of the QST-cement stone ITZ is 17.30%, which is higher than that of the FS-cement stone ITZ. However, the average pore diameter of the QST-cement stone ITZ is smaller than that of the FS. When the aperture is larger than 200 nm, the content of the macropores in the FS-cement ITZ is more than that of the QST. In the range of 50-200 nm aperture, the pore content of the QST- cement stone ITZ is more than that of the FS, indicating that the aggregate surface loading of TiO_2 refines the pore size structure of the ITZ. The content of the macropores is reduced as well. Compared with the SEM images of Fig. 10(a) and

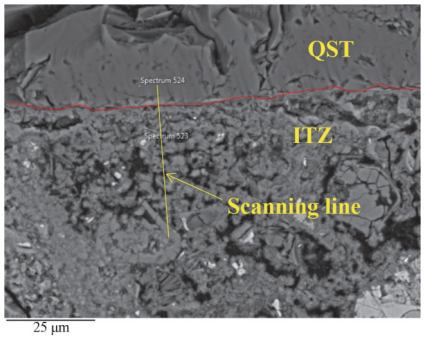

(a) SEM image of the ITZ between the QST and the cement paste

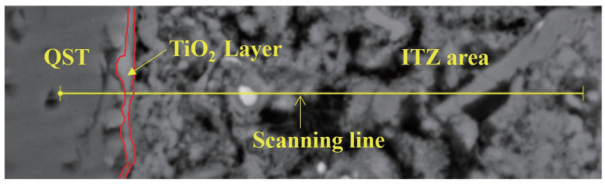

(b) SEM image of partially enlarged detail of the scanning line area

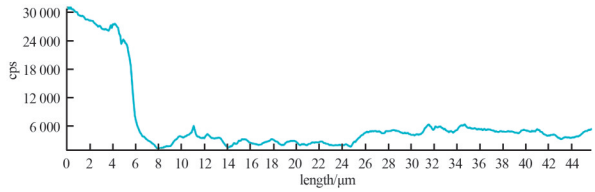

(c) the Si element content of the gap between FS particles

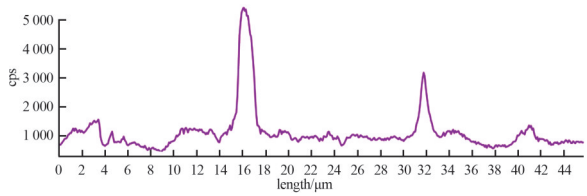

(d) the Al element content of the gap between FS particles

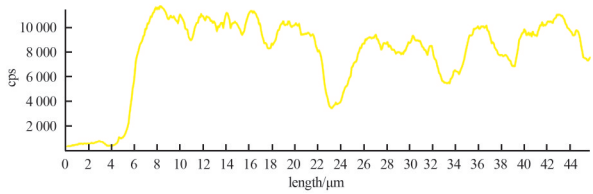

(e) the Ca element content of the gap between FS particles

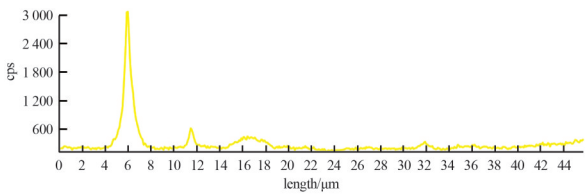

(f) the Ti element content of the gap between FS particles

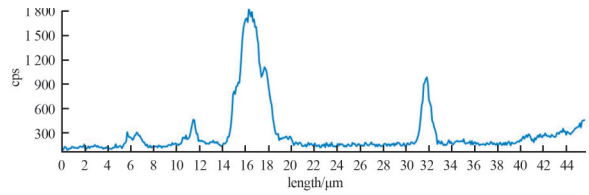

(g) the S element content of the gap between FS particles

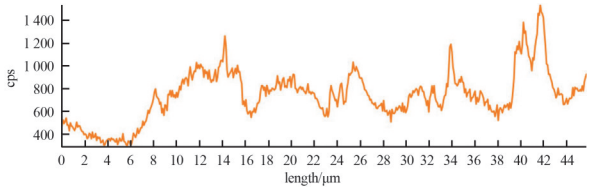

(h) the Fe element content of the gap between FS particles

Fig. 13　Line-scanning analysis of the ITZ between the QST and the cement paste

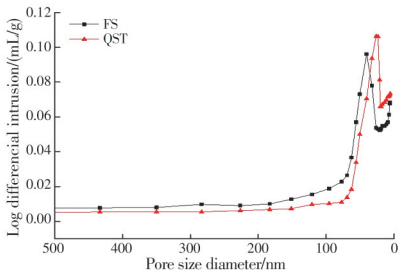

Fig. 14　Pore size distribution of the ITZ between the QST, the FS aggregates and the cement paste

Fig. 12(a), it can be concluded that the ITZ of the QST-cement paste is more compact than that of the ITZ of the FS-cement paste. The MIP test proves this result. Chen, et al. [43] and others' study has also shown that nano-TiO_2 can significantly increase the hydration level during the initial hydration stage with small content. The nucleation effect of nano-TiO_2 decreases the total porosity of the hardened cement paste, reducing the pore volume primarily occurring within the capillary.

4　Conclusion

(1) Weight loss and drying shrinkage of the FS mortar were higher than those of the QST mortar. Nano-TiO_2 particles present a pore refinement effect on the cement-based materials resulting in a much denser microstructure and lower shrinkage value. Pull-out strength of the QST mortar is higher than that of the FS mortar during the standard curing and the drying shrinkage conditions; however, the contrary result is observed under the dry-wet cycle

condition. Further investigation regarding this observation is needed in future research.

(2) The high $Ca(OH)_2$ content and porous microstructure in the FS-cement ITZ reduce the bonding strength between the FS and the cement paste. The microstructure of the ITZ between the QST and the cement paste is more compact than that of the FS. TiO_2 coated on the surface of the aggregates improves the degree of hydration of the cement and makes the microstructure dense as well as the ITZ between the aggregates and the cement.

Reference

[1] RAMIREZ A M, DEMEESTERE K, DE BELIE N, et al. Titanium dioxide coated cementitious materials for air purifying purposes: Preparation, characterization and toluene removal potential [J]. Building and Environment, 2010, 45(4): 832-838.

[2] POON C S, CHEUNG E. NO removal efficiency of photocatalytic paving blocks prepared with recycled materials [J]. Construction and Building Materials, 2007, 21(8): 1746-1753.

[3] BALLARI M M, BROUWERS H J H. Full scale demonstration of air-purifying pavement [J]. Journal of Hazardous Materials, 2013, 254/255: 406-414.

[4] BALLARI M M, HUNGER M, HÜSKEN G, et al. NO_x photocatalytic degradation employing concrete pavement containing titanium dioxide [J]. Applied Catalysis B: Environmental, 2010, 95(3/4): 245-254.

[5] ZHU Y, ZHANG J P, WANG J X, et al. Distribution and sources of air pollutants in the North China Plain based on on-road mobile measurements [J]. Atmospheric Chemistry and Physics, 2016, 16(19): 12551-12565.

[6] OCHIAI T, FUJISHIMA A. Photoelectrochemical properties of TiO_2 photocatalyst and its applications for environmental purification [J]. Journal of Photochemistry and Photobiology C: Photochemistry Reviews, 2012, 13 (4): 247-262.

[7] XU H, OUYANG S, LIU L Q, et al. Recent advances in TiO_2-based photocatalysis [J]. Journal of Materials Chemistry A, 2014, 2(32): 12642-12661.

[8] LAI Y K, HUANG J Y, CUI Z Q, et al. Recent advances in TiO_2-based nanostructured surfaces with controllable wettability and adhesion [J]. Small, 2016, 12(16): 2203-2224.

[9] FOLLI A, PADE C, HANSEN T B, et al. TiO_2 photocatalysis in cementitious systems: Insights into self-cleaning and depollution chemistry [J]. Cement and Concrete Research, 2012, 42(3): 539-548.

[10] LU Z Y, WANG Q, YIN R, et al. A novel TiO_2/foam cement composite with enhanced photodegradation of methyl blue [J]. Construction and Building Materials, 2016, 129: 159-162.

[11] YANG L, HAKKI A, WANG F Z, et al. Photocatalyst efficiencies in concrete technology: The effect of photocatalyst placement [J]. Applied Catalysis B: Environmental, 2018, 222: 200-208.

[12] FENG S L, LIU F H, FU X, et al. Photocatalytic performances and durability of TiO_2/cement composites prepared by a smear method for organic wastewater degradation [J]. Ceramics International, 2019, 45(17): 23061-23069.

[13] PRAVEENKUMAR T R, VIJAYALAKSHMI M M, MEDDAH M S. Strengths and durability performances of blended cement concrete with TiO_2 nanoparticles and rice husk ash [J]. Construction and Building Materials, 2019, 217: 343-351.

[14] MORO C, FRANCIOSO V, VELAY-LIZANCOS M. Nano-TiO_2 effects on high temperature resistance of recycled mortars [J]. Journal of Cleaner Production, 2020, 263: 121581.

[15] JIN Q, SAAD E M, ZHANG W, et al. Quantification of NO_x uptake in plain and TiO_2-doped cementitious materials [J]. Cement and Concrete Research, 2019, 122: 251-256.

[16] TRYBA B, JAFARI S, SILLANPÄÄ M, et al. Influence of TiO_2 structure on its photocatalytic activity towards acetaldehyde decomposition [J]. Applied Surface Science, 2019, 470: 376-385.

[17] CHEN K Y, LI Y, MENG X Y, et al. New integrated method to recover the TiO_2 component and prepare glass-ceramics from molten titanium-bearing blast furnace slag [J]. Ceramics International, 2019, 45(18): 24236-24243.

[18] XU M F, BAO Y, WU K, et al. Influence of TiO_2 incorporation methods on NO_x abatement in Engineered Cementitious Composites [J]. Construction and Building Materials, 2019, 221: 375-383.

[19] YANG L, HAKKI A, ZHENG L, et al. Photocatalytic concrete for NO_x abatement: Supported TiO_2 efficiencies and impacts [J]. Cement and Concrete Research, 2019, 116: 57-64.

[20] WANG F Z, YANG L, WANG H, et al. Facile preparation of photocatalytic exposed aggregate concrete with highly efficient and stable catalytic performance [J]. Chemical Engineering Journal, 2015, 264: 577-586.

[21] YANG L, HAKKI A, WANG F Z, et al. Different roles of water in photocatalytic $DeNO_x$ mechanisms on TiO_2: Basis for engineering nitrate selectivity [J]. ACS Applied Materials & Interfaces, 2017, 9(20): 17034-17041.

[22] HAKKI A, YANG L, WANG F, et al. The effect of

interfacial chemical bonding in TiO_2-SiO_2 composites on their photocatalytic NO_x abatement performance [J]. Journal of Visualized Experiments, 2017(125): 56070.

[23] BOCCI E, RIDERELLI L, FAVA G, et al. Durability of NO oxidation effectiveness of pavement surfaces treated with photocatalytic titanium dioxide [J]. Arabian Journal for Science and Engineering, 2016, 41(12): 4827-4833.

[24] GUO M Z, LING T C, POON C S. Photocatalytic NO_x degradation of concrete surface layers intermixed and spray-coated with nano-TiO_2: Influence of experimental factors [J]. Cement and Concrete Composites, 2017, 83: 279-289.

[25] DANTAS S R A, SERAFINI R, DE OLIVEIRA ROMANO R C, et al. Influence of the nano TiO_2 dispersion procedure on fresh and hardened rendering mortar properties [J]. Construction and Building Materials, 2019, 215: 544-556.

[26] RECHES Y, THOMSON K, HELBING M, et al. Agglomeration and reactivity of nanoparticles of SiO_2, TiO_2, Al_2O_3, Fe_2O_3, and clays in cement pastes and effects on compressive strength at ambient and elevated temperatures [J]. Construction and Building Materials, 2018, 167: 860-873.

[27] WANG D, HOU P K, ZHANG L N, et al. Photocatalytic activities and chemically-bonded mechanism of SiO_2@TiO_2 nanocomposites coated cement-based materials [J]. Materials Research Bulletin, 2018, 102: 262-268.

[28] KARTHIKEYAN B, DHINAKARAN G. Influence of ultrafine TiO_2 and silica fume on performance of unreinforced and fiber reinforced concrete [J]. Construction and Building Materials, 2018, 161: 570-576.

[29] GUO X, RAO L, WANG P F, et al. Photocatalytic properties of P25-doped TiO_2 composite film synthesized via Sol-gel method on cement substrate [J]. Journal of Environmental Sciences, 2018, 66: 71-80.

[30] GUO M Z, CHEN J, XIA M, et al. Pathways of conversion of nitrogen oxides by nano TiO_2 incorporated in cement-based materials [J]. Building and Environment, 2018, 144: 412-418.

[31] MISHRA A, MEHTA A, BASU S M. Clay supported TiO_2 nanoparticles for photocatalytic degradation of environmental pollutants: A review [J]. Journal of Environmental Chemical Engineering, 2018, 6(5): 6088-6107.

[32] BINAS V, PAPADAKI D, MAGGOS T, et al. Study of innovative photocatalytic cement based coatings: The effect of supporting materials [J]. Construction and Building Materials, 2018, 168: 923-930.

[33] PAUL S C, VAN ROOYEN A S, VAN ZIJL G P A G, et al. Properties of cement-based composites using nanoparticles: A comprehensive review [J]. Construction and Building Materials, 2018, 189: 1019-1034.

[34] DANIYAL M, AKHTAR S, AZAM A. Effect of nano-TiO_2 on the properties of cementitious composites under different exposure environments [J]. Journal of Materials Research and Technology, 2019, 8(6): 6158-6172.

[35] Methods of testing cement. Part 1: Determination of strength: BS EN 196-1:2005 [S]. London, UK: British Standards Institution, 2005.

[36] ZHANG R, CHENG X, HOU P K, et al. Influences of nano-TiO_2 on the properties of cement-based materials: Hydration and drying shrinkage [J]. Construction and Building Materials, 2015, 81: 35-41.

[37] SHIMOMURA T, MAEKAWA K. Micromechanical model for drying shrinkage of concrete based on the distribution function of porosity [C]// BAZANT Z P, CAROL I. Proc. 5th International RILEM Symposium on Creep and Shrinkage of Concrete, Barcelona, Spain, E & FN Spon, London, 1993: 133-139.

[38] SHIMOMURA T, MAEKAWA K. Analysis of the drying shrinkage behaviour of concrete based on the micropore structure of concrete using a micromechanical model [J]. Magazine of Concrete Research, 1997, 49 (181): 303-322.

[39] SHIMOMURA T. Modelling of initial defect of concrete due to drying shrinkage [C]//Proc. CONSEC ′98 Concrete Under Severe Conditions, Norway, 1998, 3: 2071-2083.

[40] COLLINS F, SANJAYAN J G. Effect of pore size distribution on drying shrinking of alkali-activated slag concrete [J]. Cement and Concrete Research, 2000, 30 (9): 1401-1406.

[41] DUAN P, YAN C J, LUO W J, et al. Effects of adding nano-TiO_2 on compressive strength, drying shrinkage, carbonation and microstructure of fluidized bed fly ash based geopolymer paste [J]. Construction and Building Materials, 2016, 106: 115-125.

[42] POZO-ANTONIO J S, DIONÍSIO A. Physical-mechanical properties of mortars with addition of TiO_2 nanoparticles [J]. Construction and Building Materials, 2017, 148: 261-272.

[43] CHEN J, KOU S C, POON C S. Hydration and properties of nano-TiO_2 blended cement composites [J]. Cement and Concrete Composites, 2012, 34(5): 642-649.

（编辑　胡英奎）